aerospace

MDPI

Article

Coordinated Control of Quadrotor Suspension Systems Based on Consistency Theory

Xinyu Chen [1,2,†], Yunsheng Fan [1,2,*,†], Guofeng Wang [1,2] and Dongdong Mu [1,2]

[1] College of Marine Electrical Engineering, Dalian Maritime University, Dalian 116026, China; xyc9605@hotmail.com (X.C.); gfwangsh@163.com (G.W.); ddmu@dlmu.edu.cn (D.M.)
[2] Key Laboratory of Technology and System for Intelligent Ships of Liaoning Province, Dalian 116026, China
* Correspondence: yunsheng@dlmu.edu.cn; Tel.: +86-1359-134-7650
† These authors contributed equally to this work.

Abstract: This paper designs a cooperative control method for the multi-quadrotor suspension system based on consistency theory and realizes the cooperative formation trajectory tracking control of the multi-quadrotor suspension system by designing a consistent formation cooperative algorithm of virtual piloting and a nonlinear controller. First, a new quadrotor suspension system model is established based on the traditional quadrotor model using the Newton–Euler method. This model can accurately reflect the influence of the load on the quadrotor while obtaining the swing of the load. Then, the vertical and horizontal positions are designed separately based on the quadrotor motion characteristics, and the formation algorithm based on the virtual pilot consistency theory ensures that the final convergence of each position is consistent. An integral backstepping controller and an integral backstepping sliding mode controller are designed for quadrotor position, attitude, and load swing control to achieve accurate and fast quadrotor trajectory tracking control while reducing load swing. The stability of all the controllers is demonstrated using Lyapunov functions. Finally, a multi-quadrotor suspension system formation cooperative simulation experiment is designed to verify the designed control method.

Keywords: coordinated control; leader–follower structure; quadrotor suspension system; backstepping sliding mode control; trajectory tracking

Citation: Chen, X; Fan, Y.; Wang, G.; Mu, D. Coordinated Control of Quadrotor Suspension Systems Based on Consistency Theory. *Aerospace* **2023**, *10*, 913. https://doi.org/10.3390/aerospace10110913

Academic Editor: Karim Abu Salem

Received: 21 August 2023
Revised: 16 October 2023
Accepted: 23 October 2023
Published: 26 October 2023

1. Introduction

The quadrotor suspension system is a versatile technology with diverse applications [1,2], including freight transport [3–6], agriculture, forestry, crop protection, and environmental sensing [7]. This system is highly regarded for its exceptional flight flexibility, cost effectiveness, and ease of loading and unloading [8–11]. Nevertheless, single quadrotor suspension systems have their inherent limitations, characterized by a constrained load capacity and diminished efficiency when dealing with expansive areas or multiple loads [12,13]. To surmount these limitations, the adoption of multi-quadrotor suspension systems is gaining momentum. Cooperative formation control has emerged as an enticing solution across various sectors, such as transportation and detection, capturing substantial interest among researchers [14–18]. This approach harnesses the combined capabilities of multiple quadrotors, elevating their performance and efficiency across an extensive spectrum of applications.

While there has been substantial research into the control of single quadrotor suspension systems [11,19–26], many of these methods exhibit limitations. Much of the existing research predominantly concentrates either on the load [19–21] or solely on the quadrotor [11,22,23]. Although this specialized approach ensures effective control of the individual component being studied, it often sacrifices the overall system's dynamics. This can lead to undesirable outcomes such as horizontal position oscillations of the quadrotor or significant

swings in the suspended load [24–26]. To address these issues comprehensively, there is a pressing need for integrated control strategies that simultaneously consider both the quadrotor and the suspended load. This approach aims to optimize the performance and stability of the entire system.

Multi-quadrotor suspension systems operating in coordinated formations offer several advantages, including enhanced mission efficiency, extended operational reach, and the capacity to establish networks for task execution [27]. Various formation control methods govern these systems, each with its unique strengths and approaches. Prominent among these methods are the Leader–Follower Method [28], which designates a leader quadrotor to guide the formation, albeit with potential limitations on flexibility. The Virtual Structure Method [29] introduces a virtual framework within the formation, allowing for the maintenance of desired relative positions while affording greater formation geometry flexibility. The Behavior-Based Method [30] empowers each quadrotor to exhibit specific behaviors within the formation, enhancing adaptability to dynamic environments. The Graph Theory-Based Method [31] leverages graph theory to model communication relationships among quadrotors, transforming formation control challenges into consistency and system stability problems. In recent years, there has been a notable upsurge in research centered on graph theory-based methods. These techniques, by representing communication relationships as edges in a graph, provide a potent framework for modeling multi-quadrotor systems. Through matrix transformations, they facilitate the conversion of formation control challenges into consistency and system stability problems, thereby enhancing the precision and adaptability of multi-quadrotor formation control strategies.

Consistency theory, firmly rooted in graph theory-based methodologies, stands as a fundamental concept within the domain of multi-quadrotor formation control. Its primary objective revolves around the assurance that quadrotors, operating within a formation, maintain a steadfast and unchanging relative spatial configuration as they navigate in perfect harmony and synchrony [32]. This theory assumes a central role in safeguarding the intended formation shape and preserving the relative positions of quadrotors. Consequently, it fortifies the overarching unity and stability of the formation. The bedrock of consistency theory lies in the cultivation of synchronized motion and seamless coordination among quadrotors. As a result, it profoundly enhances the efficiency and effectiveness of multi-quadrotor systems across a diverse spectrum of applications [33].

Reference [34] introduces a novel consistent formation control algorithm based on the super-twisting algorithm, notable for its robustness and effectiveness in addressing parameter uncertainties. Reference [35] combines sliding mode control and consistency theory to suppress time-varying disturbances in the position loop, ensuring that quadrotors adhere closely to desired trajectories while maintaining a fixed formation. Reference [36] tackles consistent formation control in discrete time, employing system identification techniques to obtain dynamic models for altitude, horizontal, and yaw motions of quadrotors. A consistent formation controller is designed using the Riccati equation and parameter uncertainty theorem to ensure the stable flight of multi-quadrotor formations. In contrast to the extensive research on consistent formation control of quadrotors, the field of formation flight involving quadrotor suspension systems remains relatively unexplored. Recognizing the quadrotor as the central element of the system, we propose the application of established consistent formation control techniques to quadrotor suspension systems. This extension opens new possibilities for achieving precise and coordinated control within multi-quadrotor suspension setups.

Compared to traditional quadrotor formation flight control, achieving formation with a quadrotor suspension system introduces heightened complexity and challenges [37–39]. This complexity arises from various factors, including the mutual influence between the horizontal position of the quadrotor and the oscillations of the suspended load. The introduction of two additional degrees of freedom associated with the load's swing angles necessitates innovative underdrive system control schemes. Furthermore, effective control must manage load oscillations to prevent collisions between adjacent loads. In cooperative

formation control, the unique characteristics of cable-suspended loads mandate separate handling of the horizontal direction and longitudinal height. In summary, achieving cooperative formation control in quadrotor suspension systems poses a formidable challenge due to its highly coupled, under-driven, and complex nonlinear nature. Innovative control strategies and approaches are imperative to address these challenges effectively.

Recognizing the intricate nature of quadrotor suspension systems and building upon the foundational insights from previous research that have underpinned the control of individual quadrotor suspension systems [40–42], and drawing inspiration from the field of quadrotor formation control, this paper introduces an innovative cooperative control methodology firmly rooted in the principles of consistency theory. The primary contributions and unique aspects of this study are outlined as follows:

Formation Control with a Virtual Leader: In response to the intricacies inherent to the operation of quadrotor suspension systems, this research introduces a novel formation controller, strategically incorporating a virtual leader. Deliberately designed to address both the horizontal and vertical aspects of the system, this controller places a primary emphasis on preserving the coherency of quadrotor relative positions. Notably, the design enhances the anticipated relative distances among quadrotors, effectively reducing the potential for collisions and, consequently, promoting a heightened degree of safety and synchronization within the formation.

Integrated Control for Position, Attitude, and Swing Angles: A sophisticated control strategy is meticulously devised to govern the position, attitude, and swing angles within the quadrotor suspension system. This intricate control paradigm harnesses the seamless integration of three pivotal components: the position controller, the swing angle controller, and the attitude controller. Notably, the control of swing angles in the suspension system is achieved by translating output signals from the position and swing angle controllers into inputs for the attitude controller. This holistic methodology ensures the precise tracking of quadrotor trajectories while mitigating the oscillations induced by load dynamics.

Integral Type Backstepping Sliding Mode Controller: To address the challenge posed by oscillations in the position of quadrotors induced by suspended loads, an integral-type backstepping sliding mode controller is introduced. This controller offers a resilient solution to mitigate oscillations through the skillful integration of integral control techniques within the backstepping sliding mode framework. An innovative adaptation involves substituting the conventional sign function with the hyperbolic tangent function. This alteration not only minimizes jitter in controller outputs, but also fortifies the overall robustness of the system, resulting in enhanced performance and reliability.

In summary, this paper introduces a comprehensive cooperative control framework for quadrotor suspension systems, grounded in consistency theory. The novel contributions include formation control with a virtual leader to maintain relative position coherence, an integrated control strategy covering position, attitude, and swing angles, and the implementation of an integral-type backstepping sliding mode controller with a hyperbolic tangent function for improved stability and robustness. Collectively, these innovations expand the frontiers of cooperative control for quadrotor suspension systems, tackling their inherent complexities, and laying the groundwork for more effective and reliable operations.

The specific chapters are organized as follows. Section 2 presents the dynamic modeling of the quadrotor suspension system. Section 3 shows the cooperative formation controller design and stability proof. Section 4 presents the experimental simulation results to verify the designed control scheme. Section 5 concludes the paper.

2. Quadrotor Suspension System Dynamic

The quadrotor suspension system includes a quadrotor body with six degrees of freedom and a suspended load with two degrees of freedom, which cannot simply be

treated as the drive of the load or the load as a disturbance to the quadrotor, so a new quadrotor suspension system model must be established. The model is shown in Figure 1.

In Figure 1, a common cross-type quadrotor is shown, defining the inertial coordinate system $O_I\{X_I, Y_I, Z_I\}$. The center of mass of the quadrotor is considered as the origin of the quadrotor body coordinate system [5], x points in the direction of the tail of the aircraft, y points to the right of the aircraft, the z vertical xoy plane points above the aircraft body, α is the angle between the cable and the xoz plane, β is the angle between the cable and the yoz plane, and the cable length is L. The conversion of inertial and airframe coordinate systems is described by Euler angles, the rotation around the x-axis is the roll angle ϕ, the rotation around the y-axis is the pitch angle θ, the rotation around the z-axis is the yaw angle ψ. The rotation matrix is

$$\boldsymbol{R}_B^I = \begin{bmatrix} c\theta c\psi & s\phi s\theta\, c\psi - c\phi s\psi & -s\phi\, s\psi - c\phi s\theta c\psi \\ c\theta s\psi & s\phi s\theta\, s\psi + c\phi c\psi & s\phi\, c\psi - c\phi s\theta s\psi \\ -s\theta & s\phi c\theta & c\phi\, c\theta \end{bmatrix}, \tag{1}$$

where s means sin and c means cos.

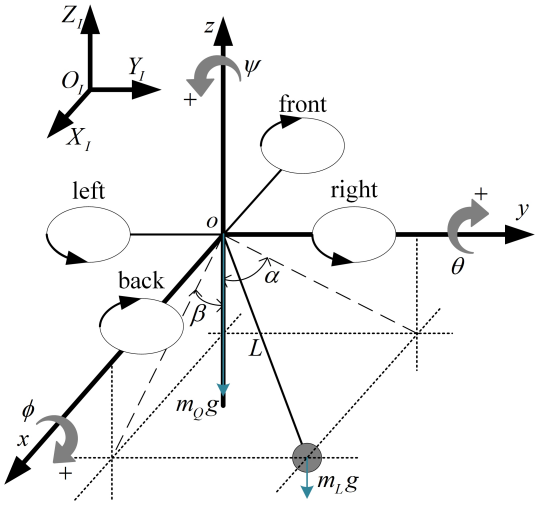

Figure 1. Quadrotor suspension system model.

We define the position of the quadrotor as $\boldsymbol{\xi} = [x, y, z]^T$, the attitude of the quadrotor as $\Theta = [\phi, \theta, \psi]^T$, the swing angle of the load as $\boldsymbol{\delta} = [\alpha, \beta]^T$. The cable attachment point is considered to be the center of mass of the quadrotor, and the cable is considered to be tight at all times. Considering that the load is always under the quadrotor, that is, $-90^\circ < \alpha, \beta < 90^\circ$.

The system is driven by a quadrotor motor, the rotor generates lift T_i and reaction-torque Q_i, $i = 1, 2, 3, 4$, and the control signal $\boldsymbol{U}_B$ is

$$\boldsymbol{U}_B = \begin{bmatrix} U_1 \\ U_2 \\ U_3 \\ U_4 \end{bmatrix} = \begin{bmatrix} T_1 + T_2 + T_3 + T_4 \\ T_3 - T_4 \\ T_2 - T_1 \\ Q_1 + Q_2 - Q_3 - Q_4 \end{bmatrix}. \tag{2}$$

Since the load cable is assumed to be tied to the quadrotor's center of mass, the load is assumed to have no effect on the quadrotor's attitude angle, so we model the attitude dynamics using the Newton–Euler equation.

$$\boldsymbol{I}_Q \dot{\boldsymbol{\varsigma}} + \boldsymbol{\varsigma} \times (\boldsymbol{I}_Q \boldsymbol{\varsigma}) = \boldsymbol{M}_a, \tag{3}$$

where $\boldsymbol{I}_Q = diag(I_x, I_y, I_z)$ is the rotational inertia and $\boldsymbol{\varsigma} = [p, q, r]^T$ is the attitude angular velocity. Using the principle of small-angle approximation, we let $\boldsymbol{\varsigma} = \Theta$, $\boldsymbol{M}_a = [lU_2, lU_3; U_4]^T$ is external moments, l is the quadrotor arm length.

The positions of the quadrotor and the swing angle are coupled, so we use the Euler–Lagrange function to model the dynamics.

The position of the load $\boldsymbol{\xi}_L = [x_L, y_L, z_L]^T$ can be obtained from the quadrotor position and the swing angle, with cable length

$$\boldsymbol{\xi}_L = \boldsymbol{\xi} + L\boldsymbol{\rho}, \tag{4}$$

where $\boldsymbol{\rho} = \begin{bmatrix}\rho_1\\ \rho_2\\ \rho_3\end{bmatrix} = \begin{bmatrix}\sin\beta\\ \sin\alpha\cos\beta\\ -\cos\alpha\cos\beta\end{bmatrix}$.

The Euler–Lagrange function is as follows, and $\boldsymbol{q} = [x, y, z, \alpha, \beta]^T$,

$$L(\boldsymbol{q}, \dot{\boldsymbol{q}}) = T(\boldsymbol{q}, \dot{\boldsymbol{q}}) - V(\boldsymbol{q}), \tag{5}$$

where $T(\boldsymbol{q}, \dot{\boldsymbol{q}}) = T_Q + T_L$ is system kinetics composed of quadrotor kinetic energy T_Q and load kinetic energy T_L, $V(\boldsymbol{q})$ is the potential energy of the system.

The kinetic energy of the system is

$$T(\boldsymbol{q}, \dot{\boldsymbol{q}}) = \frac{1}{2}m_Q\dot{\boldsymbol{\xi}}^T\dot{\boldsymbol{\xi}} + \frac{1}{2}m_L\dot{\boldsymbol{\xi}}_L^T\dot{\boldsymbol{\xi}}_L, \tag{6}$$

where m_Q, m_L are quadrotor and load mass.

System potential energy is

$$V(\boldsymbol{q}) = m_Q g z + m_L g z_L. \tag{7}$$

We obtain the Euler–Lagrange equations for system

$$\frac{d}{dt}\left(\frac{\partial L(\boldsymbol{q}, \dot{\boldsymbol{q}})}{\partial \dot{\boldsymbol{q}}}\right) - \frac{\partial L(\boldsymbol{q}, \dot{\boldsymbol{q}})}{\partial \boldsymbol{q}} = \boldsymbol{F}_g, \tag{8}$$

where $\boldsymbol{F}_g = \left[\boldsymbol{F}_p^T, \boldsymbol{M}_s^T\right]^T$ is the internal and external forces and moments on the system, and $\boldsymbol{F}_p = \left[\boldsymbol{R}_B^I[0, 0, U_1] - [0, 0, (m_Q + m_L)g]\right]^T$, $\boldsymbol{M}_s = [0, 0]^T$. Substituting $\boldsymbol{q} = [x, y, z, \alpha, \beta]^T$, we can obtain the quadrotor suspension system position and the swing angle model.

In summary, we can obtain the dynamics model of the quadrotor suspension system.

$$\begin{cases} \ddot{\phi} = \frac{lU_2}{I_x} + \frac{I_y - I_z}{I_x}\dot{\theta}\dot{\psi} \\ \ddot{\theta} = \frac{lU_3}{I_y} + \frac{I_z - I_x}{I_y}\dot{\phi}\dot{\psi} \\ \ddot{\psi} = \frac{U_4}{I_z} + \frac{I_x - I_y}{I_z}\dot{\phi}\dot{\theta} \\ \ddot{x} = \frac{a_1U_1 - m_L L b_1}{m_Q + m_L} \\ \ddot{y} = \frac{a_2U_1 - m_L L b_2}{m_Q + m_L} \\ \ddot{z} = \frac{a_3U_1 - m_L L b_3}{m_Q + m_L} - g \\ \ddot{\alpha} = \frac{c_1 - (\cos\alpha a_2 + \sin\alpha a_3)U_1}{m_Q L\cos\beta} \\ \ddot{\beta} = \frac{c_2 - (\cos\beta a_1 + \sin\beta\sin\alpha a_2 + \sin\beta\cos\alpha a_3)U_1}{m_Q L} \end{cases}, \tag{9}$$

where $\begin{cases} a_1 = -\sin\phi\sin\psi - \cos\phi\sin\theta\cos\psi \\ a_2 = \sin\phi\cos\psi - \cos\phi\sin\theta\sin\psi \\ a_3 = \cos\phi\cos\theta \end{cases}$, $\begin{cases} b_1 = \frac{\partial^2\rho_1}{\partial t^2} \\ b_2 = \frac{\partial^2\rho_2}{\partial t^2} \\ b_3 = \frac{\partial^2\rho_3}{\partial t^2} \end{cases}$, $\begin{cases} c_1 = 2m_Q L\sin\beta\dot{\beta}\dot{\alpha} \\ c_2 = -m_Q L\sin\beta\cos\beta^2 \end{cases}$.

3. Cooperative Formation Controller Design

The cooperative formation controller in this paper is divided into a trajectory generation part based on consistency theory and a nonlinear controller part based on integral type backstepping sliding mode, and the control block diagram is shown in Figure 2.

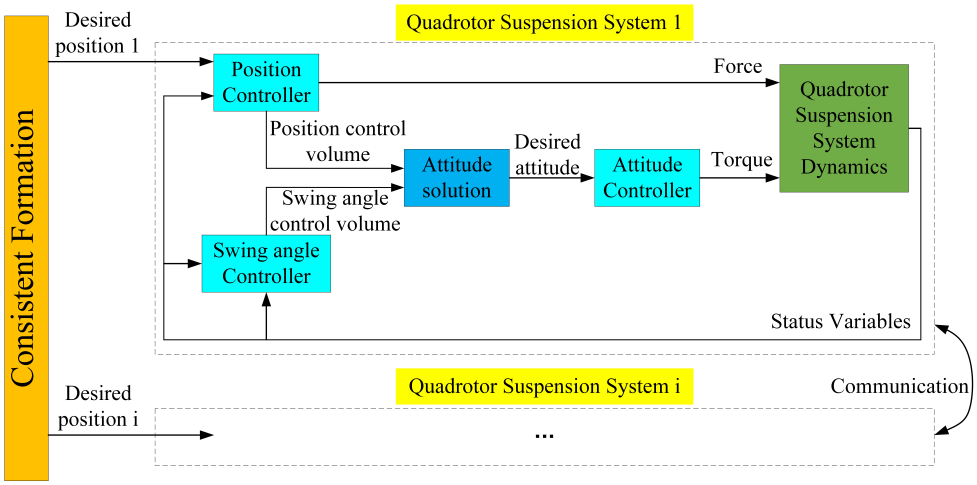

Figure 2. Cooperative formation and backstepping sliding mode control structure.

In Figure 2, the desired trajectory for each quadrotor is computed using the first-order consistent formation system, employing virtual piloting. The control parameters u_x, u_y, u_α, and u_β are derived from both the position controller and the swing angle controller. Notably, for the attitude solution, the influence of roll and pitch on position is disregarded, that is, $\begin{cases} \phi_d = (u_y + u_\beta)\cos\psi - (u_x + u_\alpha)\sin\psi \\ \theta_d = -(u_y + u_\beta)\sin\psi - (u_x + u_\alpha)\cos\psi \end{cases}$. The desired attitude is obtained, and the force and moment of the system are obtained by the attitude angle controller and position controller to realize the trajectory tracking control of the quadrotor suspension system.

The control structure designed in this paper has the advantage of converting the control quantity of the swing angle controller to the attitude control input, thus avoiding the problem of start failure caused by the conversion to the position control input, and at the same time realizing the accurate control of the quadrotor position and the swing reduction control of the suspended load.

3.1. Collaborative Trajectory Generation

In the context of ensuring the consistent formation control of multi-quadrotor suspension systems, a fundamental understanding of algebraic graph theory is indispensable. Let us define an oriented graph $G = \{V, E\}$, where the vertex set is denoted as $V = \{v_1, v_2, \ldots, v_n\}$, representing a collection of n nodes, and the edge set is $E \subseteq V \times V$, signifying the adjacency relationships between these nodes. The index set for the nodes is denoted as $I \in \{1, 2, \ldots, n\}$. To describe the communication relationships among the nodes, we introduce the adjacency matrix $A = \{a_{ij}\} \in R^{n\times n}$. Here, the element a_{ij} takes on the value > 0 to indicate that node j can receive information from node i, while $a_{ij} = 0$ signifies the absence of such information flow. Furthermore, the Laplacian matrix of G is defined as $L_A = \{l_{ij}\} \in R^{n\times n}$, with diagonal elements $l_{ii} = \sum_{j=1}^{n} a_{ij}$ and off-diagonal elements $l_{ij} = -a_{ij}$.

Theorem 1 ([43]). *For a communication structure directed graph G consisting of n intelligent agents, a sufficient necessary condition for this system to converge to average consistency, which means that the states or behaviors of these agents collectively tend to reach a specific consistent state or value, is that graph G is a strongly connected equilibrium graph or a connected undirected graph.*

The first-order consistent formation control algorithm with navigator designed in this paper, i.e., the consistency of the quadrotor positions, thus considers the agents as single-integral systems with the equation of state

$$\dot{\xi}_i = u_i, i = 1, 2, \cdots, n, \tag{10}$$

where $\xi_i \in R$ is the position state of agent i, and $u_i \in R$ is the control input.

Theorem 2 ([43]). *In any initial state, the control algorithm u_i enables the multi-agent system (10) to satisfy*

$$\lim_{t\to\infty} \left|\xi_i - \xi_j\right| = 0, i = 1, 2, \cdots, n. \tag{11}$$

Then, the multi-intelligent body system (10) is said to be able to achieve asymptotic consistency.

The design consistency formation algorithm is

$$u_i = -h(\xi_i - \xi_i^* - \xi_0) - \left(\sum_{j=1}^{n} a_{ij}\left[(\xi_i - \xi_i^*) - \left(\xi_j - \xi_j^*\right)\right]\right), \tag{12}$$

where h denotes the communication relationship between the virtual navigator and the follower, $h = 1$ is the ability of the follower to receive information from the navigator, $\boldsymbol{\xi}^* \in R$ is the deviation matrix related to system formation, and $\boldsymbol{\xi}_0 \in R$ is the position state of the navigator. From Theorem 2, it can be seen that the designed algorithm can make the intelligent body agree while maintaining the relative distance from the navigator.

We propose a virtual pilot and six quadrotor followers. Each follower can obtain the information of the pilot, and the directed communication topology is shown in Figure 3.

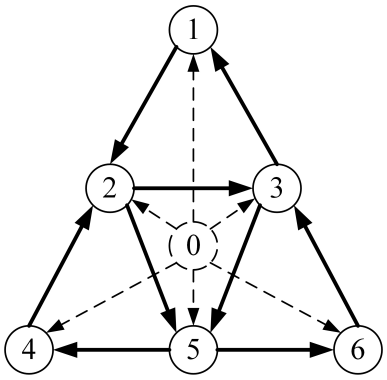

Figure 3. Quadrotor suspension system communication topology.

The communication graph in Figure 3 is a strongly connected graph containing a directed spanning tree. The adjacency matrix is $\mathbf{A} = \begin{bmatrix} 0 & 1 & 1 & 1 & 1 & 1 & 1 \\ 0 & 0 & 1 & 0 & 0 & 0 & 0 \\ 0 & 0 & 0 & 1 & 0 & 1 & 0 \\ 0 & 1 & 0 & 0 & 0 & 1 & 0 \\ 0 & 0 & 1 & 0 & 0 & 0 & 0 \\ 0 & 0 & 0 & 0 & 1 & 0 & 1 \\ 0 & 0 & 0 & 1 & 0 & 0 & 0 \end{bmatrix}$, the

Laplacian matrix is $\mathbf{L} = \begin{bmatrix} 6 & -1 & -1 & -1 & -1 & -1 & -1 \\ 0 & 1 & -1 & 0 & 0 & 0 & 0 \\ 0 & 0 & 2 & -1 & 0 & -1 & 0 \\ 0 & -1 & 0 & 2 & 0 & -1 & 0 \\ 0 & 0 & -1 & 0 & 1 & 0 & 0 \\ 0 & 0 & 0 & 0 & -1 & 2 & -1 \\ 0 & 0 & 0 & -1 & 0 & 0 & 1 \end{bmatrix}$. From Theorem 1, the system is consistent.

3.2. Controller Design

The controller design of the quadrotor suspension system is divided into three modules: quadrotor attitude, quadrotor position, and suspension swing angle, where attitude is the inner loop and position and suspension swing angle are the outer loop. In the following, $k_\bullet$,$\lambda_\bullet$,$\mu_\bullet$, $h_\bullet$ and $\varepsilon_\bullet$ are all constants greater than zero. First, the integral type backstepping controller is designed. We take the roll angle ϕ as an example.

Step 1: Define the error

$$e_\phi = \phi_d - \phi, \tag{13}$$

where ϕ_d is the desired roll angle, deriving Equation (13) and obtaining the error of the roll angle velocity

$$\dot{e}_\phi = \dot{\phi}_d - \dot{\phi} = \dot{\phi}_d - w_\phi \tag{14}$$

where w_ϕ is the virtual input volume.

Step 2: Design the Lyapunov function of e_ϕ:

$$V_1 = \frac{1}{2} e_\phi^2. \tag{15}$$

The derivative is obtained as

$$\dot{V}_1 = e_\phi \dot{e}_\phi = e_\phi (\dot{\phi}_d - w_\phi). \tag{16}$$

Take w_ϕ as the virtual control input, i.e., the actual roll speed, and define its expected value as $w_{\phi d}$ to make $\dot{V}_1 \leq 0$; let $w_{\phi d} = k_\phi e_\phi + \dot{\phi}_d$.

Step 3: Add an integration term to the desired virtual input to increase robustness and reduce error:

$$w_{\phi d} = k_\phi e_\phi + \dot{\phi}_d + \lambda_\phi \chi_\phi, \tag{17}$$

where $\chi_\phi = \int_0^t e_\phi(\tau) d\tau$.

Step 4: Define the virtual input error

$$e_{\dot{\phi}} = w_{\phi d} - w_\phi. \tag{18}$$

Substituting in $w_{\phi d}$, we obtain

$$w_\phi = k_\phi e_\phi + \dot{\phi}_d + \lambda_\phi \chi_\phi - e_{\dot{\phi}}. \tag{19}$$

The derivative of (18) can be obtained as

$$\dot{e}_{\dot{\phi}} = \dot{w}_{\phi d} - \dot{w}_\phi = k_\phi \dot{e}_\phi + \ddot{\phi}_d + \lambda_\phi e_\phi - \ddot{\phi}, \tag{20}$$

where $\ddot{\phi}$ is a roll angle acceleration model. It can be obtained from (19),

$$\dot{V}_1 = e_\phi (\dot{\phi}_d - w_\phi) = -k_\phi e_\phi^2 - e_\phi \lambda_\phi \chi_\phi + e_\phi e_{\dot{\phi}}. \tag{21}$$

To make $\dot{V}_1 \leq 0$, it is also needed to make $e_{\dot{\phi}}$, χ_ϕ tend to zero.

Step 5: Design Lyapunov functions for e_ϕ, $e_{\dot\phi}$, χ_ϕ:

$$V_2 = \frac{1}{2}e_\phi^2 + \frac{1}{2}e_{\dot\phi}^2 + \frac{1}{2}\lambda_\phi\chi_\phi^2. \tag{22}$$

Differentiate (22)

$$\dot V_2 = e_\phi\dot e_\phi + e_{\dot\phi}\dot e_{\dot\phi} + \lambda_\phi\chi_\phi\dot\chi_\phi. \tag{23}$$

Substitute (20) and (21) into (23):

$$\dot V_2 = -k_\phi e_\phi^2 + e_\phi e_{\dot\phi} + e_{\dot\phi}\left(k_\phi\dot e_\phi + \ddot\phi_d + \lambda_\phi e_\phi - \frac{lU_2 + \dot\theta\dot\psi(I_y - I_z)}{I_x}\right). \tag{24}$$

To make $\dot V_2 \le 0$, design the control variable U_2 as

$$U_2 = \frac{I_x}{l}\left[\left(1 - k_\phi^2 + \lambda_\phi\right)e_\phi + \left(k_\phi + k_{\dot\phi}\right)e_{\dot\phi} - k_\phi\lambda_\phi\chi_\phi + \ddot\phi_d - \frac{\dot\theta\dot\psi(I_y - I_z)}{I_x}\right]. \tag{25}$$

The proof of the stability of the integral type backstepping controller is as follows:

Proof. Taking U_2 into (24), we can obtain

$$\dot V_2 = -k_\phi e_\phi^2 - k_{\dot\phi}e_{\dot\phi}^2 \le 0. \tag{26}$$

It can be concluded that the designed control law is asymptotically stable. □

Similarly, the control laws for pitch angle and yaw angle can be obtained, along with stability proof.

$$U_3 = \frac{I_y}{l}\left[\left(1 - k_\theta^2 + \lambda_\theta\right)e_\theta + \left(k_\theta + k_{\dot\theta}\right)e_{\dot\theta} - k_\theta\lambda_\theta\chi_\theta + \ddot\theta_d - \frac{\dot\phi\dot\psi(I_z - I_x)}{I_y}\right], \tag{27}$$

$$U_4 = I_z\left[\left(1 - k_\psi^2 + \lambda_\psi\right)e_\psi + \left(k_\psi + k_{\dot\psi}\right)e_{\dot\psi} - k_\psi\lambda_\psi\chi_\psi + \ddot\psi_d - \frac{\dot\phi\dot\theta(I_x - I_y)}{I_z}\right], \tag{28}$$

where θ_d, ψ_d represent the desired pitch angle and yaw angle, respectively, and

$$\begin{cases} e_\theta = \theta_d - \theta, \chi_\theta = \int_0^t e_\theta(\tau)d\tau \\ e_{\dot\theta} = k_\theta e_\theta + \dot\theta_d + \lambda_\theta\chi_\theta - \dot\theta \\ e_\psi = \psi_d - \psi, \chi_\psi = \int_0^t e_\psi(\tau)d\tau \\ e_{\dot\psi} = k_\psi e_\psi + \dot\psi_d + \lambda_\psi\chi_\psi - \dot\psi \end{cases}.$$

Similarly, the swing angle controller is designed in the same manner.

$$\begin{cases} u_\alpha = \dfrac{m_Q L\cos\beta\left[\left(1 - k_\alpha^2 + \lambda_\alpha\right)e_\alpha + \ddot\alpha_d + (k_\alpha + k_{\dot\alpha})e_{\dot\alpha} - k_\alpha\lambda_\alpha\chi_\alpha\right] + c_1}{U_1} \\ u_\beta = \dfrac{m_Q L\left[\left(1 - k_\beta^2 + \lambda_\beta\right)e_\beta + \ddot\beta_d + \left(k_\beta + k_{\dot\beta}\right)e_{\dot\beta} - k_\beta\lambda_\beta\chi_\beta\right] + c_2}{U_1} \end{cases}, \tag{29}$$

where $\ddot\alpha_d$ and $\ddot\beta_d$ are the desired values, and the definitions of each variable that appear are as follows: $\begin{cases} e_\alpha = \alpha_d - \alpha, \chi_\alpha = \int_0^t e_\alpha(\tau)d\tau \\ e_{\dot\alpha} = k_\alpha e_\alpha + \dot\alpha_d + \lambda_\alpha\chi_\alpha - \dot\alpha \\ s_\alpha = \mu_\alpha e_\alpha + e_{\dot\alpha} \end{cases}$, $\begin{cases} e_\beta = \beta_d - \beta, \chi_\beta = \int_0^t e_\beta(\tau)d\tau \\ e_{\dot\beta} = k_\beta e_\beta + \dot\beta_d + \lambda_\beta\chi_\beta - \dot\beta \\ s_\beta = \mu_\beta e_\beta + e_{\dot\beta} \end{cases}$.

The position of the quadrotor is susceptible to disturbances and load. Therefore, an integral backstepping sliding mode controller is designed by combining sliding mode control with backstepping control to address this issue. Taking the altitude z of the quadrotor as an example, the first four steps are the same as mentioned above.

Step 1: Define the error term $e_z = z_d - z$ and the virtual input w_z.

Step 2: Design a Lyapunov function $V_1 = \frac{1}{2}e_z^2$ for the error term e_z such that the desired virtual input is $w_{zd} = k_z e_z + \dot{z}_d$.

Step 3: Add an integral term to the function $w_{zd} = k_z e_z + \dot{z}_d + \lambda_z \chi_z$, $\chi_z = \int_0^t e_z(\tau)d\tau$.

Step 4: Define the error term for the virtual input $e_{\dot{z}} = w_{zd} - w_z = k_z e_z + \dot{z}_d + \lambda_z \chi_z - \dot{z}$.

Step 5: Based on the integral backstepping method, add sliding mode control and define the sliding surface.

$$s_z = \mu_z e_z + e_{\dot{z}} = (\mu_z + k_z)e_z + \dot{e}_z + \lambda_z \chi_z. \tag{30}$$

Taking the derivative of s_z,

$$\dot{s}_z = \mu_z \dot{e}_z + \dot{e}_{\dot{z}} = (\mu_z + k_z)(e_{\dot{z}} - k_z e_z - \lambda_z \chi_z) + \lambda_z e_z + \ddot{z}_d - \frac{a_3 U_1 - m_L L b_3}{m_Q + m_L} + g. \tag{31}$$

Step 6: Design Lyapunov functions for e_z, χ_z, s_z:

$$V_2 = \frac{1}{2}e_z^2 + \frac{1}{2}\lambda_\phi \chi_\phi^2 + \frac{1}{2}s_z^2. \tag{32}$$

Taking the derivative of (32),

$$\begin{aligned} \dot{V}_2 &= e_z \dot{e}_z + \lambda_z \chi_z \dot{\chi}_z + s_z \dot{s}_z \\ &= -k_z e_z^2 + e_z e_{\dot{z}} + s_z \begin{bmatrix} (\mu_z + k_z)(e_{\dot{z}} - k_z e_z - \lambda_z \chi_z) + \\ \lambda_z e_z + \ddot{z}_d - \dfrac{a_3 U_1 - m_L L b_3}{m_Q + m_L} + g \end{bmatrix}. \end{aligned} \tag{33}$$

To make the controller stable and reduce chattering in sliding mode control, use the hyperbolic tangent function instead of the sign function and design the control law.

$$U_1 = \frac{(m_Q + m_L)\begin{bmatrix} (\mu_z + k_z)(e_{\dot{z}} - k_z e_z - \lambda_z \chi_z) \\ + \lambda_z e_z + \ddot{z}_d + g + h_z s_z + \varepsilon_z \tanh(s_z) \end{bmatrix} + m_L L b_3}{a_3}; \tag{34}$$

ε_z is the sliding mode switching gain.

The proof of the stability of the integral backstepping sliding mode controller is as follows:

Proof. Substituting (34) into (33),

$$\begin{aligned} \dot{V}_2 &= -k_z e_z^2 + e_z e_{\dot{z}} + s_z[-h_z s_z - \varepsilon_z \tanh(s_z)] \\ &\leq -k_z e_z^2 + e_z e_{\dot{z}} - h_z s_z^2 - \varepsilon_z |s_z| \end{aligned}. \tag{35}$$

We let Q be a positive definite matrix.

$$Q = \begin{bmatrix} k_z + h_z \mu_z^2 & h_z \mu_z - \frac{1}{2} \\ h_z \mu_z - \frac{1}{2} & h_z \end{bmatrix}. \tag{36}$$

The determinant of Q is positive, which means the control parameters need to satisfy $h_z(k_z + \mu_z) - \frac{1}{4} > 0$. We can obtain

$$\begin{aligned} &\begin{bmatrix} e_z \\ e_{\dot{z}} \end{bmatrix}^T \begin{bmatrix} k_z + h_z \mu_z^2 & h_z \mu_z - \frac{1}{2} \\ h_z \mu_z - \frac{1}{2} & h_z \end{bmatrix} \begin{bmatrix} e_z \\ e_{\dot{z}} \end{bmatrix}. \\ &= k_z e_z^2 - e_z e_{\dot{z}} + h_z s_z^2 \end{aligned} \tag{37}$$

We substitute into (35)

$$\dot{V}_2 \leq -\begin{bmatrix} e_z \\ e_{\dot{z}} \end{bmatrix}^T Q \begin{bmatrix} e_z \\ e_{\dot{z}} \end{bmatrix} - \varepsilon_z |s_z| \leq 0. \tag{38}$$

Therefore, it can be proved that the control system is stable. □

Similarly, horizontal position controllers and swing angle controllers can be designed. It should be noted that the horizontal position controller does not directly obtain the desired roll and pitch angles, but obtains the desired rotation matrix, that is, $\begin{cases} u_x = a_1 \\ u_y = a_2 \end{cases}$, to avoid the calculation of inverse sine and greatly reduce the computational complexity. The design process and stability analysis are not repeated here, and the results are obtained.

$$\begin{cases} u_x = \dfrac{(m_Q+m_L)\begin{bmatrix} (\mu_x + k_x)(e_{\dot{x}} - k_x e_x - \lambda_x \chi_x) \\ +\lambda_x e_x + \ddot{x}_d + h_x s_x + \varepsilon_x \tanh(s_x) \end{bmatrix} + m_L L b_1}{U_1} \\ u_y = \dfrac{(m_Q+m_L)\begin{bmatrix} (\mu_y + k_y)(e_{\dot{y}} - k_y e_y - \lambda_y \chi_y) \\ +\lambda_y e_y + \ddot{y}_d + h_y s_y + \varepsilon_y \tanh(s_y) \end{bmatrix} + m_L L b_2}{U_1} \end{cases}, \tag{39}$$

where $\ddot{x}_d$ and $\ddot{y}_d$ are the desired values, and the definitions of each variable that appear are as follows: $\begin{cases} e_x = x_d - x, \chi_x = \int_0^t e_x(\tau) d\tau \\ e_{\dot{x}} = k_x e_x + \dot{x}_d + \lambda_x \chi_x - \dot{x} \\ s_x = \mu_x e_x + e_{\dot{x}} \end{cases}$, $\begin{cases} e_y = y_d - y, \chi_y = \int_0^t e_y(\tau) d\tau \\ e_{\dot{y}} = k_y e_y + \dot{y}_d + \lambda_y \chi_y - \dot{y} \\ s_y = \mu_y e_y + e_{\dot{y}} \end{cases}$.

4. Simulation Results

This paper employs Simulink simulation experiments to validate the proposed control scheme. The model parameters for the quadrotor suspension system are shown in Table 1.

Table 1. Model Parameters for the Quadrotor Suspension System.

Parameter	Value
m_Q	1.8 kg
m_L	0.2 kg
l	0.2 m
I_x	0.03 kg·m^2
I_y	0.03 kg·m^2
I_z	0.04 kg·m^2
g	9.81 m/(s^2)
L	0.3 m

The initial positions of the six quadrotors are $\xi_0 = \begin{bmatrix} 0 & -1 & 1 & -2 & 0 & 2 \\ 0 & -1 & -1 & -2 & -2 & -2 \\ 0 & 0 & 0 & 0 & 0 & 0 \end{bmatrix}^T$, with position deviation matrix $\xi^* = \begin{bmatrix} 0 & -1.5 & 1.5 & -3 & 0 & 3 \\ 2\sqrt{3} & \sqrt{3}/2 & \sqrt{3}/2 & -\sqrt{3} & -\sqrt{3} & -\sqrt{3} \\ 0 & 0 & 0 & 0 & 0 & 0 \end{bmatrix}^T$. The trajectory of the virtual leader is $\begin{cases} 0, t > 0 \\ 0, t > 0 \\ 3, t > 0 \end{cases}$, $\begin{cases} 0.3(t-10), t > 10 \\ 2\sin 0.3(t-10), t > 10 \\ 3, t > 10 \end{cases}$, with the first 10 s being the rising stage. The control system parameters are shown in Table 2.

Table 2. Control System Model Parameters.

Parameter	Value
$k_{\phi,\theta}$, k_{ψ}, $k_{x,y}$, k_{z},$k_{\alpha,\beta}$	53.3, 5.8, 1.45, 7.8, 1
$k_{\dot{\phi},\dot{\theta}}$, $k_{\dot{\psi}}$, $k_{\dot{\alpha},\dot{\beta}}$	5.5, 3.5, 2
$\lambda_{\phi,\theta}$, λ_{ψ}, $\lambda_{x,y}$, λ_{z}, $\lambda_{\alpha,\beta}$	8.5, 0.01, 0.015, 20.55, 0.1
$\mu_{x,y}$, μ_{z}	0.5, 20
$h_{x,y}$, h_{z}	0.8, 1
$\varepsilon_{x,y}$, ε_{z}	2, 5

The following are the results of the simulation experiments.

The expected trajectory of the quadrotor generated by the consensus formation algorithm shown in Figure 4. It can be observed from the figure that the designed formation algorithm can effectively complete the formation task under the guidance of the virtual leader, generating a formation trajectory that brings the quadrotors' horizontal and vertical positions from the initial position to the expected formation trajectory. Additionally, the algorithm forms the corresponding formation according to the designed deviation matrix and maintains consistency among the quadrotors.

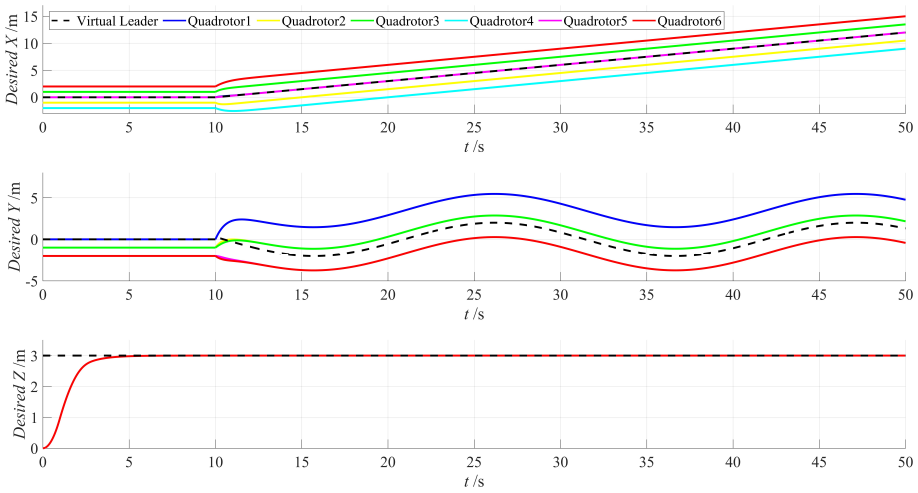

Figure 4. Consistent formation-generated quadrotor desired trajectories.

Figures 5–7 illustrate the flight trajectories of six quadrotor suspension systems controlled by the designed method, backstepping control, and PID control, respectively. It is evident that all three methods enable the quadrotors to reach the desired altitude and successfully track their respective planned formation paths. Consequently, they achieve coordinated control of the multi-quadrotor suspension system. Nevertheless, variations in position control accuracy exist among these methods.

Figures 8 and 9 illustrate the position errors of the quadrotors using the three control methods. It is clear that, when compared to the control without the swing angle controller, the method proposed in this paper achieves stability within 5 s, while the backstepping method takes 10 s, and PID control requires 15 s. Furthermore, the approach outlined in this paper exhibits a smaller overshoot. Once stability is reached, the positions of the quadrotors are influenced by load swinging due to the absence of a swing angle controller. As a result, periodic errors persist even after stability is achieved, and this issue remains unresolved with the backstepping method, while PID control induces more significant oscillations. However, the design presented in this paper significantly mitigates the impact of load swinging, preventing the repetitive oscillation of quadrotor positions.

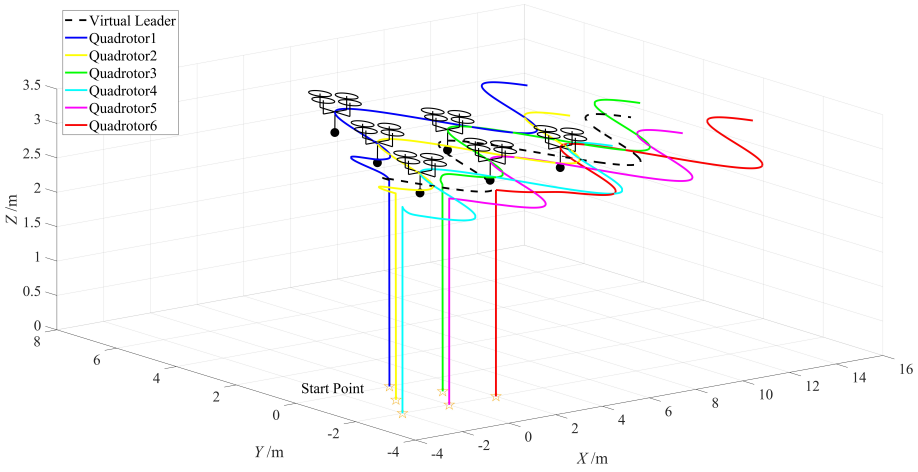

Figure 5. 3D trajectories under proposed method.

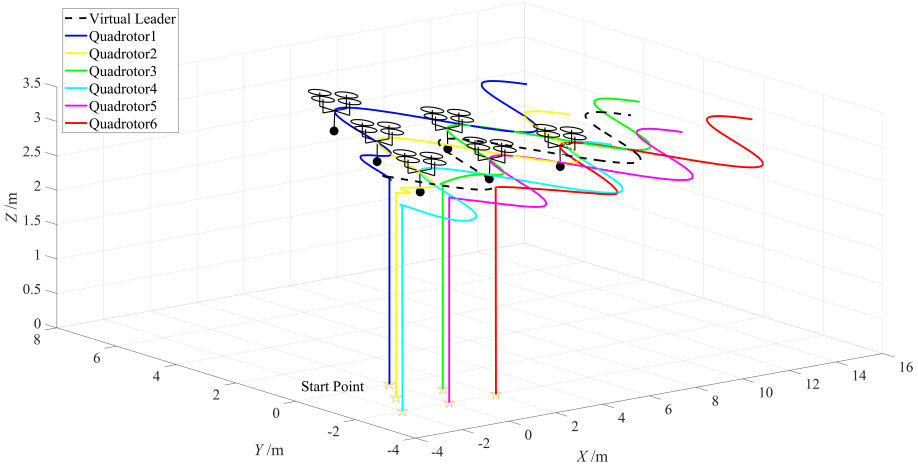

Figure 6. 3D trajectories through Backstepping controller without swing angle controller.

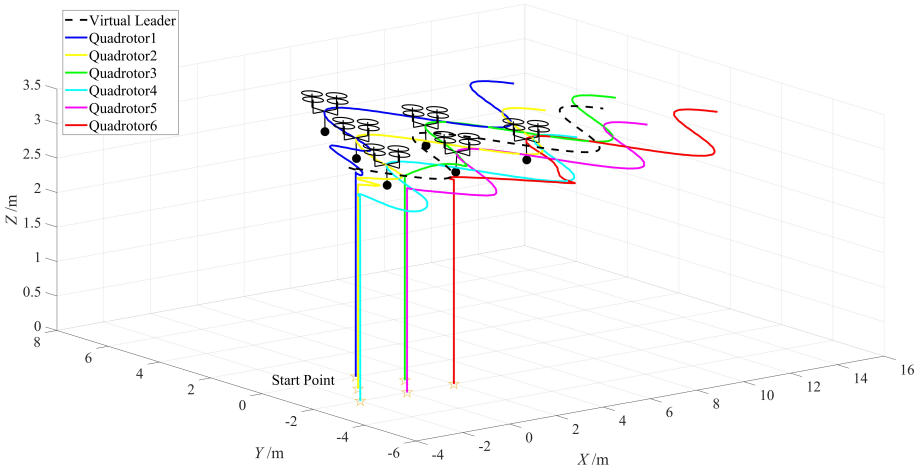

Figure 7. 3D trajectories through PID controller without swing angle controller.

Figure 10 illustrates the swinging of the suspended load under the three control methods. It is evident that, with the swing angle controller in place, the suspended load experiences smaller swings when the quadrotor initiates horizontal movement and quickly achieves stability. Minimal swings occur as the quadrotor's position undergoes periodic motion, with the absence of high-frequency oscillations. This design effectively mitigates the risks associated with excessive and frequent load swings.

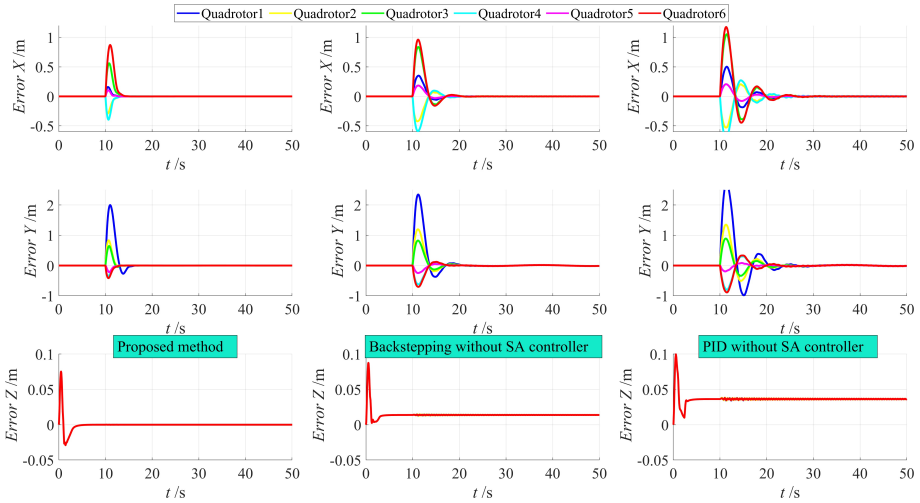

Figure 8. Position control error of 6 quadrotors throughout the process.

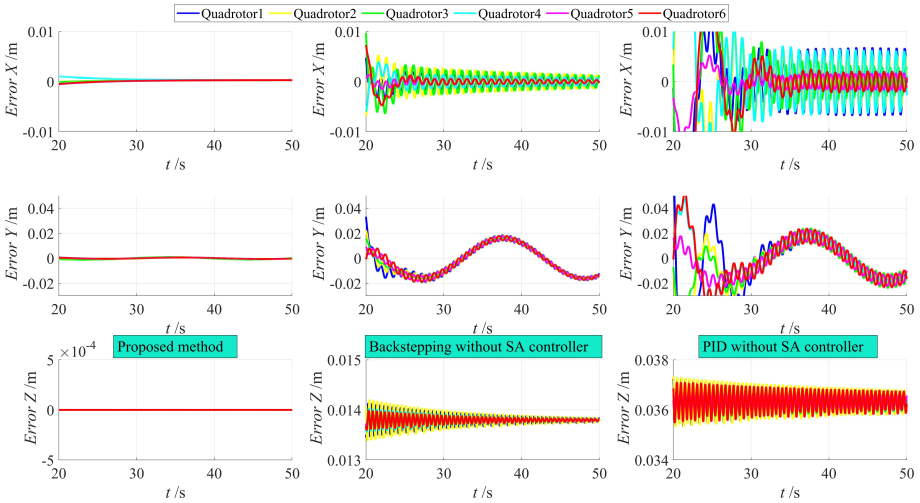

Figure 9. Control error of 6 quadrotors after 20 s.

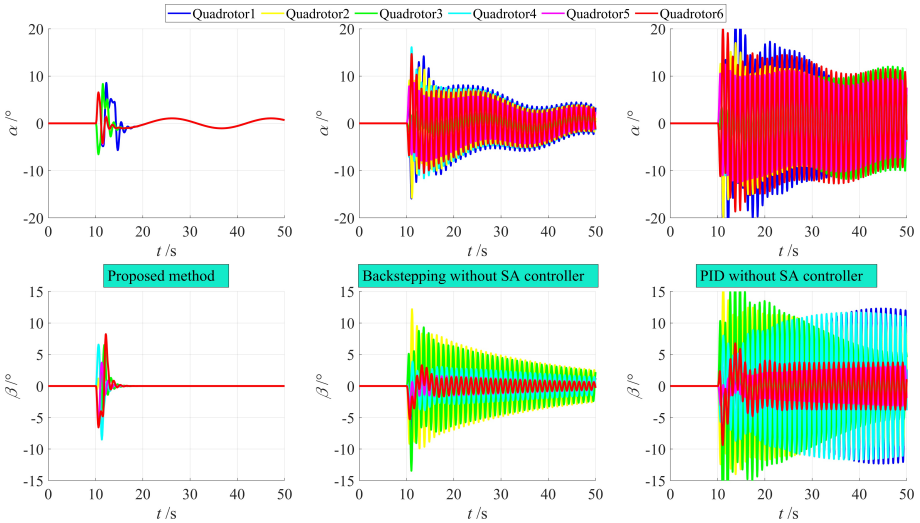

Figure 10. Comparison of swing angles under different control methods.

Figure 11 shows the control of the quadrotor's attitude angles. It can be observed that the control method designed in this paper can accurately and quickly track the desired attitude angles.

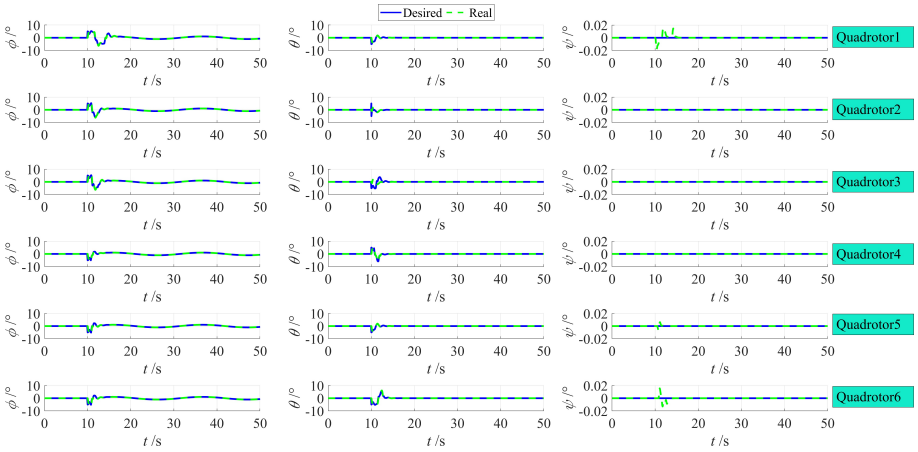

Figure 11. Desired and real attitude angle control.

5. Conclusions

To solve the problem of coordinated control of quadrotor suspension systems, this paper proposes a nonlinear control method based on a consistency algorithm and backstepping sliding mode control. An accurate eight-degree-of-freedom dynamic model of the quadrotor suspension system is established using the Lagrangian equation. A consistency formation algorithm with a virtual leader is designed to plan the formation flight trajectory of multiple quadrotor suspension systems. To address the issue of the quadrotor position being sensitive to load swinging, an integral backstepping sliding mode controller is designed for the quadrotor position channel, while integral backstepping controllers are designed for the quadrotor attitude and load swinging. By converting the output values of the outer-loop position and swinging controllers into the inner-loop attitude reference values, the control method not only achieves quadrotor trajectory tracking control, but also suppresses load swinging. Finally, simulation experiments using Simulink are conducted to verify the effectiveness of the proposed control method, which outperforms the backstepping control method in terms of control accuracy and load swinging suppression.

Author Contributions: Conceptualization, G.W. and X.C.; methodology, X.C.; software, X.C.; validation, D.M.; formal analysis, Y.F.; investigation, X.C.; resources, G.W.; data curation, D.M.; writing—original draft preparation, X.C.; writing—review and editing, X.C.; visualization, D.M.; supervision, D.M.; project administration, G.W.; funding acquisition, Y.F. All authors have read and agreed to the published version of the manuscript.

Funding: This research was funded by "the Nature Science Foundation of China" (grand number61976033, 51609033), "the Nature Science Foundation of Liaoning Province of China" (grand number 20180520005), "the Fundamental Research Funds for the Central Universities" (grand numbers 3132021106, 3132020110), "the Liaoning Province Doctoral Research Start-up" (grand number 2022-BS-094), "the China Postdoctoral Science Foundation" (grand number 2022M710569) and "the postgraduate education and teaching reform project of Dalian Maritime University" (grand number YJG2022713).

Data Availability Statement: The data presented in this study are available on request from the corresponding author. The data are not publicly available due to privacy.

Acknowledgments: This work was supported by "the Nature Science Foundation of China" (grand number61976033, 51609033), "the Nature Science Foundation of Liaoning Province of China" (grand number 20180520005), "the Fundamental Research Funds for the Central Universities" (grand numbers 3132021106, 3132020110), "the Liaoning Province Doctoral Research Start-up" (grand number 2022-BS-094), "the China Postdoctoral Science Foundation" (grand number 2022M710569) and "the postgraduate education and teaching reform project of Dalian Maritime University" (grand number YJG2022713).

Conflicts of Interest: The authors declare no conflict of interest.

References

1. Jiang, B.; Li, B.; Zhou, W.; Lo, L.-Y.; Chen, C.-K.; Wen, C.-Y. Neural Network Based Model Predictive Control for a Quadrotor UAV. *Aerospace* **2022**, *9*, 460. [CrossRef]
2. Mariani, M.; Fiori, S. Design and Simulation of a Neuroevolutionary Controller for a Quadcopter Drone. *Aerospace* **2023**, *10*, 418. [CrossRef]
3. Potter, J.J.; Adams, C.J.; Singhose, W. A planar experimental remote-controlled helicopter with a suspended load. *IEEE/ASME Trans. Mechatronics* **2015**, *20*, 2496–2503. [CrossRef]
4. Duan, D.; Wang, Z.; Li, J.; Zhang, C.; Wang, Q. Stabilization control for unmanned helicopter-slung load system based on active disturbance rejection control and improved sliding mode control. *Proc. Inst. Mech. Eng. Part G J. Aerosp. Eng.* **2021**, *235*, 1803–1816. [CrossRef]
5. Yang, S.; Xian, B.; Cai, J.; Wang, G. Finite-time convergence control for a quadrotor unmanned aerial vehicle with a slung load. *IEEE Trans. Ind. Inform.* 2023, *early access*.
6. Outeiro, P.; Cardeira, C.; Oliveira, P. Control Architecture for a Quadrotor Transporting a Cable-Suspended Load of Uncertain Mass. *Drones* **2023**, *7*, 201. [CrossRef]
7. Si, P.; Fu, Z.; Shu, L.; Yang, Y.; Huang, K.; Liu, Y. Target-barrier coverage improvement in an insecticidal lamps internet of UAVs. *IEEE Trans. Veh. Technol.* **2022**, *71*, 4373–4382. [CrossRef]
8. Sreenath, K.; Lee, T.; Kumar, V. Geometric control and differential flatness of a quadrotor UAV with a cable-suspended load. In Proceedings of the 52nd IEEE Conference on Decision and Control, Firenze, Italy, 10–13 December 2013; pp. 2269–2274.
9. Vahdanipour, M.; Khodabandeh, M. Adaptive fractional order sliding mode control for a quadrotor with a varying load. *Aerosp. Sci. Technol.* **2019**, *86*, 737–747. [CrossRef]
10. Wang, Z.; Zhao, T. Based on robust sliding mode and linear active disturbance rejection control for attitude of quadrotor load UAV. *Nonlinear Dyn.* **2022**, *108*, 3485–3503. [CrossRef]
11. Roy, K.R.; Waghmare, L.M.; Patre, B.M. Dynamic modeling and displacement control for differential flatness of quadrotor UAV slung-load system. *Int. J. Dyn. Control.* **2023**, *11*, 637–655. [CrossRef]
12. Yang, P.; Zhang, A.; Bi, W.; Li, M. Cooperative group formation control for multiple quadrotors system with finite-and fixed-time convergence. *ISA Trans.* **2023**, *138*, 186–196. [CrossRef]
13. Doakhan, M.; Kabganian, M.; Azimi, A. Robust adaptive control for formation-based cooperative transportation of a payload by multi quadrotors. *Eur. J. Control.* **2023**, *69*, 100763. [CrossRef]
14. Zhang, K.; Yang, Z.; Başar, T. Multi-agent reinforcement learning: A selective overview of theories and algorithms. In *Handbook of Reinforcement Learning and Control*; Springer: Berlin/Heidelberg, Germany, 2021; pp. 321–384.
15. Oroojlooy, A.; Hajinezhad, D. A review of cooperative multi-agent deep reinforcement learning. *Appl. Intell.* **2023**, *53*, 13677–13722. [CrossRef]
16. Du, Z.; Negenborn, R.R.; Reppa, V. Cooperative multi-agent control for autonomous ship towing under environmental disturbances. *IEEE/CAA J. Autom. Sin.* **2021**, *8*, 1365–1379. [CrossRef]
17. Mukras, S.M.S.; Omar, H.M. Development of a 6-DOF testing platform for multirotor flying vehicles with suspended loads. *Aerospace* **2021**, *8*, 355. [CrossRef]
18. Ding, F.; Sun, C.; Ai, Y.; Huang, J. Sliding Mode Control for Quadrotor-Slung Load Transportation System with State Constraints. In Proceedings of the 2022 IEEE International Conference on Cyborg and Bionic Systems (CBS), Wuhan, China, 24–26 March 2023; pp. 368–373.
19. Yu, G.; Cabecinhas, D.; Cunha, R.; Silvestre, C. Aggressive maneuvers for a quadrotor-slung-load system through fast trajectory generation and tracking. *Auton. Robot.* **2022**, *46*, 499–513. [CrossRef]
20. Lv, Z.; Zhao, Q.; Li, S.; Wu, Y. Finite-time control design for a quadrotor transporting a slung load. *Control. Eng. Pract.* **2022**, *122*, 105082. [CrossRef]
21. Lv, Z.; Wu, Y.; Sun, X.-M.; Wang, Q.-G. Fixed-time control for a quadrotor with a cable-suspended load. *IEEE Trans. Intell. Transp. Syst.* **2022**, *23*, 21932–21943. [CrossRef]
22. Salih, Z.; Saleh, M.H. Attitude and Altitude Control of Quadrotor Carrying a Suspended Payload using Genetic Algorithm. *J. Eng.* **2022**, *28*, 25–40. [CrossRef]
23. Sun, H.; Gu, X.; Luo, S.; Liang, Y.; Bai, J. Robust stabilization technique for a quadrotor slung-load system using sliding mode control. *J. Phys. Conf. Ser.* **2022**, *2232*, 012013. [CrossRef]
24. Chandra, A.; Lal, P.P.S. Higher Order Sliding Mode Controller for a Quadrotor UAV with a Suspended Load. *IFAC-PapersOnLine* **2022**, *55*, 610–615. [CrossRef]
25. Wang, J.; Yuan, X.; Zhu, B. Geometric control for trajectory-tracking of a quadrotor UAV with suspended load. *IET Control. Theory Appl.* **2022**, *16*, 1271–1281. [CrossRef]
26. Omar, H.M.; Mukras, S. Integrating anti-swing controller with px4 autopilot for quadrotor with suspended load. *J. Mech. Sci. Technol.* **2022**, *36*, 1511–1519. [CrossRef]
27. Yan, D.; Zhang, W.; Chen, H. Design of a multi-constraint formation controller based on improved MPC and consensus for quadrotors. *Aerospace* **2022**, *9*, 94. [CrossRef]
28. Wang, P.K.C. Navigation strategies for multiple autonomous mobile robots moving in formation. *J. Robot. Syst.* **1991**, *8*, 177–195. [CrossRef]

29. Lewis, M.A.; Tan, K.H. High precision formation control of mobile robots using virtual structures. *Auton. Robot.* **1997**, *4*, 387–403. [CrossRef]
30. Balch, T.; Arkin, R.C. Behavior-based formation control for multirobot teams. *IEEE Trans. Robot. Autom.* **1998**, *14*, 926–939. [CrossRef]
31. Desai, J.P.; Ostrowski, J.P.; Kumar, V. Modeling and control of formations of nonholonomic mobile robots. *IEEE Trans. Robot. Autom.* **2001**, *17*, 905–908. [CrossRef]
32. Liu, R.; Qu, B.; Wei, T.; Zhang, L.; Yan, L.; Chai, X. Research on UAV Formation Obstacle Avoidance Based on Consistency Control. In Proceedings of the 2023 IEEE 12th Data Driven Control and Learning Systems Conference (DDCLS), Xiangtan, China, 12–14 May 2023; pp. 155–160.
33. Yu, H.; Ning, L. Coordinated Obstacle Avoidance of Multi-AUV Based on Improved Artificial Potential Field Method and Consistency Protocol. *J. Mar. Sci. Eng.* **2023**, *11*, 1157. [CrossRef]
34. Rojo-Rodriguez, E.G.; Garcia, O.; Ollervides, E.J.; Zambrano-Robledo, P.; Espinoza-Quesada, E.S. Robust consensus-based formation flight for multiple quadrotors. *J. Intell. Robot. Syst.* **2019**, *93*, 213–226. [CrossRef]
35. Wang, J.; Ma, X.; Li, H.; Tian, B. Self-triggered sliding mode control for distributed formation of multiple quadrotors. *J. Frankl. Inst.* **2020**, *357*, 12223–12240. [CrossRef]
36. Steinleitner, A.; Ballam, R.; McFadyen, A. Practical consensus-based formation control for quadrotor systems. In Proceedings of the 2022 International Conference on Unmanned Aircraft Systems (ICUAS), Dubrovnik, Croatia, 21–24 June 2022; pp. 1510–1519.
37. Liu, Y.; Li, Y. Application of Inverse Optimal Formation Control for Euler-Lagrange Systems. *IEEE Trans. Intell. Transp. Syst.* **2023**, *24*, 5655–5662. [CrossRef]
38. Hwang, C.L.; Abebe, H.B. Generalized and heterogeneous nonlinear dynamic multiagent systems using online RNN-based finite-time formation tracking control and application to transportation systems. *IEEE Trans. Intell. Transp. Syst.* **2021**, *23*, 13708–13720. [CrossRef]
39. Omar, H.M.; Akram, R.; Mukras, S.M.S.; Mahvouz, A.A. Recent advances and challenges in controlling quadrotors with suspended loads. *Alex. Eng. J.* **2023**, **63**, 253–270. [CrossRef]
40. Chen, X.; Zhao, Y.; Fan, Y. Adaptive Integral Backstepping Control for a Quadrotor with Suspended Flight. In Proceedings of the 2020 5th International Conference on Automation, Control and Robotics Engineering (CACRE), Dalian, China, 19–20 September 2020; pp. 226–234.
41. Fan, Y.; Guo, H.; Han, X.; Chen, X. Research and Verification of Trajectory Tracking Control of a Quadrotor Carrying a Load. *Appl. Sci.* **2022**, *12*, 1036. [CrossRef]
42. Fan, Y.; Chen, X.; Zhao, Y.; Song, B. Nonlinear control of quadrotor suspension system based on extended state observer. *Acta Autom. Sin.* **2023**, *49*, 1758–1770.
43. Olfati-Saber, R.; Fax, J.A.; Murray, R.M. Consensus and cooperation in networked multi-agent systems. *Proc. IEEE* **2007**, *95*, 215–233. [CrossRef]